MAPPING THE IRON OXIDATION STATE IN MARTIAN METEORITES. A. M. Martin[1], [1]Lunar and Planetary Institute (amartin@lpi.usra.edu), A. H. Treiman[1] (treiman@lpi.usra.edu), and K. Righter[2], [2]NASA Johnson Space Center (kevin.righter-1@nasa.gov).

Introduction: Several types of Martian igneous meteorites have been identified: clinopyroxenites (nakhlites), basaltic shergottites, peridotitic shergottites, dunites (chassignites) and orthopyroxenites [1,2]. In order to constrain the heterogeneity of the Martian mantle and crust, and their evolution through time, numerous studies have been performed on the iron oxidation state of these meteorites [3,4,5,6,7,8,9]. The calculated fO_2 values all lie within the FMQ-5 to FMQ+0.5 range (FMQ representing the Fayalite = Magnetite + Quartz buffer); however, discrepancies appear between the various studies, which are either attributed to the choice of the minerals/melts used, or to the precision of the analytical/calculation method.

The redox record in volcanic samples is primarily related to the oxidation state in the mantle source(s). However, it is also influenced by several deep processes: melting, crystallization, magma mixing [10], assimilation and degassing [11]. In addition, the oxidation state in Martian meteorites is potentially affected by several surface processes: assimilation of sediment/crust during lava flowing at Mars' surface, low temperature micro-crystallization [10], weathering at the surface of Mars and low temperature re-equilibration, impact processes (i.e. high pressure phase transitions, mechanical mixing, shock degassing and melting), space weathering, and weathering on Earth (at atmospheric conditions different from Mars).

Decoding the redox record of Martian meteorites, therefore, requires large-scale quantitative analysis methods, as well as a perfect understanding of oxidation processes.

Method: Recent XAFS measurements on volcanic samples from Earth highlight Fe redox zoning in anisotropic minerals such as olivine and pyroxene [12]. We run similar analyses on Martian meteorites of various types, in order to (1) reveal the potential redox heterogeneities, (2) explain the discrepancies between previous studies and (3) constrain the role of late processes, in particular, shock melting and alteration, on the redox record of the Martian igneous history. We mapped the iron oxidation variations in minerals from four meteorites: MIL03346 (olivine and clinopyroxene), ALH 77005 (orthopyroxene), ALH84001 (pyroxene), Tissint (olivine, pyroxene, amphibole). Analyses were run on synchrotron at the Advanced Photon Source (GSECARS 13-ID-E). Fluorescence maps were acquired at selected energies (2-4 µm step size), and processed to remove the effect of total Fe content. We used oriented standards to lower the analytical error [12,13,14,15,16]. Point analyses were also acquired at selected locations (white dots on Figs. 1,2, and 3), and treated using the same method as [13].

Results and Discussion:

MIL03346 (nakhlite). This meteorite has a clinopyroxenite composition. It has been explained by the fractional crystallization of a magma on Mars [17]. The presence of volatiles (especially carbon) in its mantle source has been proposed [5,7] to explain its high oxidation state [4].

We run two iron redox maps, one on an altered olivine, one on a zoned clinopyroxene crystal. The presence of highly oxidized forms of olivine (e.g., laihunite) has been reported in the Yamato 00 nakhlites [18]. Ferric saponite and serpentine have also been found in nakhlites olivines [19]. Iddingiste-like veins have been observed in MIL03346 [17,20]. In our olivine from MIL03346, we observed numerous oxidation veins. In the non-oxidized parts of the crystal, Fe^{3+}/Fe is lower than 10 %, but reaches extremely high values similar to laihunite and "oxyfayalite" [21] in some veins.

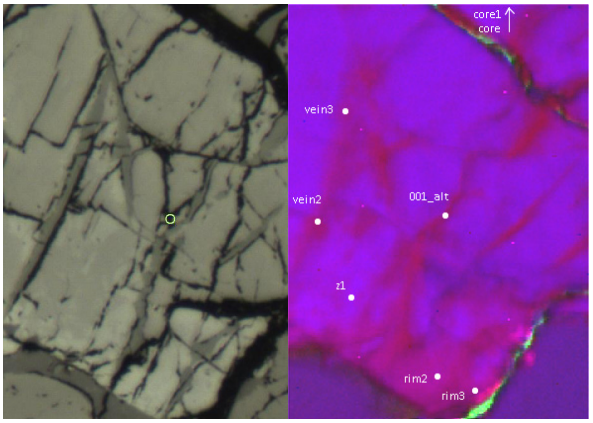

Figure 1. (Left) Reflected-light optical image of an altered olivine in MIL03346. (Right) Iron oxidation map of the same crystal (R=Fe^{3+}, B=Fe^{2+}, G=1/Fe). Image width ~300 µm.

The iron oxidation map of the clinopyroxene crystal shows several oxidation features, including a thin oxidized rim, micro variations inside the crystal, and an oxidation rim around an inclusion.

ALH77005 (Lherzolitic shergottite). Spinels from this meteorite have been studied to constrain its oxidation state [3]. We focused on the transition from brown to colorless minerals near an impact vein. Our analyses show that this transition corresponds to a decrease in Fe^{3+}/Fe fraction. This may be due to some devolatilization during the impact melting event.

Tissint (Olivine-phyric basaltic shergottite). The oxidation variations during the crystallization of this sample have been studied by [9]. They concluded that the rock was first reduced, then oxidized during cooling. The presence of impact melt veins, and high pressure minerals, has been described by [22]. Our iron oxidation map shows an increase in the Fe^{3+}/Fe fraction close to and inside the impact veins. This is likely due to the incompatible nature of volatiles.

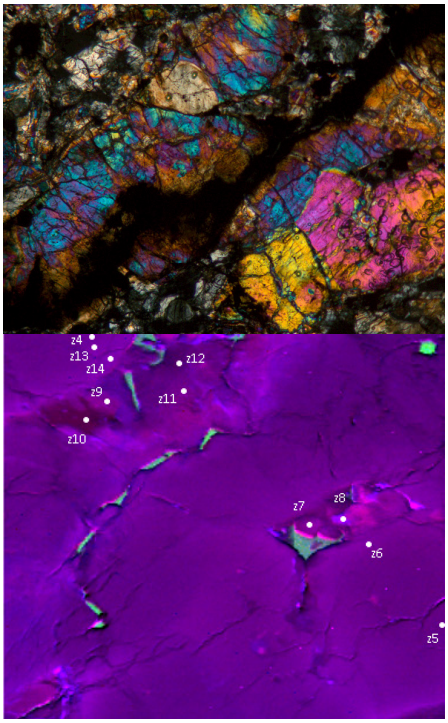

Figure 2. (Up) Cross polarized light image of an impact melt vein from Tissint (in black). (Down) Iron oxidation map of the same region. Image width ~1 mm.

ALH84001 (Orthopyroxenite). This meteorite, which has been suspected to contain evidence for fossil life on Mars, is mainly composed of orthopyroxene, chromite and olivine. It underwent multiple schock events [23], and presents numerous impact veins. Our analyses show that the Fe^{3+}/Fe content is higher inside and near the veins, like in Tissint.

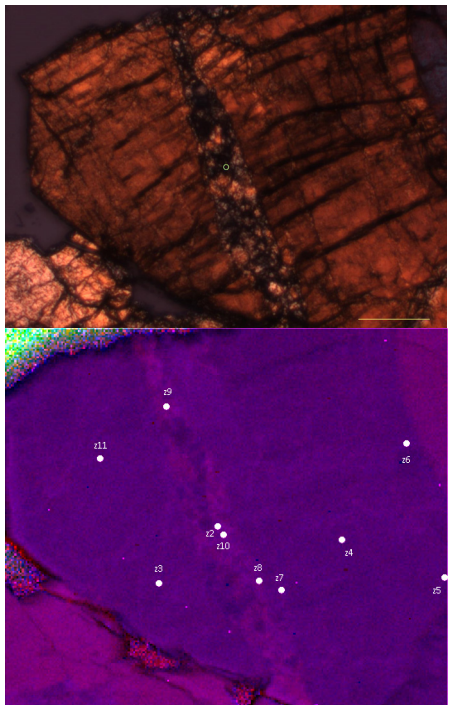

Figure 3. (Up) Transmitted light optical image of an impact melt vein in a pyroxene from ALH84001. (Down) Iron oxidation map of the same region. Image width ~1.1 mm.

References:

[1] Bridges J.C. and Warren P.H. (2006) *JGS, London, 163,* 229-251. [2] Papike et al. (2009) *GCA, 73,* 7443-7485. [3] Goodrich C. et al. (2003) *MAPS, 38,* 1773-1792. [4] Dyar M.D. et al (2005) *JGR, 110,* E09005. [5] Righter K. et al. (2008) *MAPS, 43,* 1709-1723. [6] McCanta M.C. et al. (2009) *MAPS, 44,* 725-745. [7] Martin A.M. and Righter K. (2013) *CMP, 166(4),* 1067-1098. [8] Righter K. et al. (2013) *AmMin, 98,* 616-628. [9] Castle N. and Herd C.D.K. (2016) *MAPS,* 1-22. [10] Herd C.D.K. et al. (2016) *LPSC 47,* Abstract #2527. [11] Kelley and Cottrell (2012) *EPSL, 329-330,* 109-121. [12] Martin A.M. et al. (2016) *LPSC 47,* Abstract #3059. [13] Martin A.M. et al. (submitted) *Lithos.* [14] Berry A.J. et al. (2013) *Geology, 41,* 683-686. [15] Cottrell E. et al. (2009) *Chem. Geol., 268,* 167-179. [16] McCanta M.C. et al (2004) *AmMin, 89,* 1685-1693. [17] Treiman A.H. (2005) *Chemie Der Erde, 65,* 203-270. [18] Noguchi T. et al. (2009) *JGR, 114,* E10004. [19] Hicks L.J. et al. (2014) *GCA, 136,* 194-210. [20] Stopar J.D. et al. (2013) *GCA, 112,* 208-225. [21] Martin A.M. et al. (2015) *AmMin, 100,* 1153-1164. [22] Walton et al (2014) *GCA, 140,* 334-348. [23] Treiman A.H. (1998) *MAPS, 33,* 753-764.